https://erjm.journals.ekb.eg
ISSN: 1110-1180

DOI: ---------

ERJ
Engineering Research Journal
Faculty of Engineering
Menoufia University

Surface Quality and Phase Analysis of Hot-Forged Carbon Boron Steel Using Abbott Firestone Technique

Abeer S. Eisa[1*], Ahmed M. Elfaramawy[1], Ahmed R. Desouky[1], Ahmed I. Farahat[2]

[1]Department of Production Eng., Faculty of Eng., Menoufia University, Egypt.
[2]Central Metallurgical Research Institute (CMRDI), Cairo, Egypt
**(Corresponding author: Drabeereisa78@yahoo.com)*

ABSTRACT

Carbon boron steels exhibit outstanding mechanical properties at a low price. The carbon steel's mechanical properties are increased by adding micro additives such as boron and titanium, which satisfy automotive industry needs. Steel grades S355J2 and 27MnCrB5 rolled bars were hot-forged at 1200°C with a reduction in cross-sectional area of about 60%. The hot-forged samples were air-cooled. Dilatation measurements were carried out to determine the critical transformation temperatures. The mechanical properties were evaluated using the tensile test. The effect of micro additives, especially boron, was studied on continuous and discontinuous yielding behavior. Microstructure investigation was carried out using optical and scanning electron microscopes (SEM). A new technique has been used to determine the volume fraction of different phases. It depends on surface roughness deduced from optical or SEM micrographs to construct the Abbott Firestone curve. Abbott Firestone curve technique results are reliable and very close to that Image j software results with a percentage of 95%.

Keywords*: Boron Steel, Dilatation, Abbott Firestone curve, Discontinuous Yielding*

1. INTRODUCTION

From an economic point of view, boron was added to steel, as it is an effective and less expensive alternative compared to the other elements such as Mn or Cr or Mo or Ni in terms of hardenability, it is possible to dispense with adding (in wt. %) 0.6 Mn or 0.7 Cr or 0.5 Mo or 1.5 Ni by adding 10–30 wt. Ppm of protected boron to steel in terms of hardenability [1-3]. Boron inhibits the nucleation of ferrite on austenitic grain boundaries and thereby enhances martensite formation by shifting the C-curves to the right, i.e., longer times, thereby improving the hardenability of the steel [3,4]. Boron is used to make a high grain refining via increasing the non-recrystallization temperature during hot deformation, which prevents the grain growth after finishing hot deformation, especially at high temperature, so it is useful for the production of forged parts with a fine-grained microstructure [5]. Boron acts as a micro-alloying element in steel which affects the ferrite volume fraction and thickness, therefore, affecting the forged part's final mechanical properties [6,7]. Microstructural components such as ferrite and austenite grain size, precipitates, and texture, have their pronounced effect on the strength and toughness of control rolled micro-alloyed steels [8]. Abbott Firestone curve is a valuable technique used to look for specific tribological characteristics, whereas the traditional roughness parameters such as Ra (average surface roughness) or Rq (the root mean square of the surface roughness) can't provide information about surface nature [9]. Abbott Firestone curve makes it possible to conceive the distribution of the heights of the peaks and valleys in the profile, thereby obtaining qualitative and quantitative qualitative criteria for enhancing the selection of work system, material, and manufacturing processes [9, 10]. In this work, the boron effect on intercritical zones (partial transformation from ferrite to austenite) and phase thickness have been studied. A new technique to determine the volume fraction of different phases depending on surface roughness deduced from optical or SEM micrographs is used. Each phase has its own signature, represented in the heights of the peaks and valleys; hence, the Abbott curve was adapted to determine the volume fraction, then compared its results with the image j software result.

2. EXPERIMENTAL DETAILS

2.1. Steel alloys manufacturing

Steel alloys were casted using a continuous casting machine in ARCOSTEEL Company, Sadat City-Egypt for Special Steel. The chemical composition was adjusted well, especially the boron element since it reacts readily with the oxygen and nitrogen and forms useless compounds in the steel, So oxygen and nitrogen scavengers elements such as titanium,,aluminum and silicon which have a greater affinity to oxygen and nitrogen than does

boron were added to the liquid steel before adding boron [3]. Their percentages are given in Table 1. Casted billets were hot rolled and then were hot-forged at 1200°C, and air cooling was applied to decrease the grain size and to control the final size of samples, as shown in Fig. 1. Emission Spectroscopy (OES 3460) was used for elemental analyses.

2.2. Dilatation

Dilatation samples were machined to Φ4 × 30 mm, as shown in Fig. 2. Measurements were carried out with a heating rate of 10°C/s to determine the temperatures of the critical transformation (Ac1, Ac3, Ms, Md, Bs, and Bf) from the dilatation curves, and the data are given in Table 2.

2.3. Microstructure investigation

After performing the hot-forging process, the samples were cut and prepared by nitric etching and polishing. Microstructure investigation was carried out using optical Axioplan Universal Microscope and scanning electron microscope**.**

2.4. Tensile testing

The specimens for the tensile test were prepared according to ASTME8/E8M and carried out using Universal Testing Machine (UH-500 KNX-R) to determine the mechanical properties (strength and elongation) after hot-forging.

Table 1: Chemical composition of as forged alloys determined by Optical Emission Spectroscopy

Alloy No	Steel grade	C	Si	Mn	P	S	Ni	Cr	Mo	Cu	AL	Ca (ppm)	Ti	B	Fe
1	**S355j2**	0.19	0.41	1.42	0.037	0.018	0.08	0.11	0.02	0.20	0.021	17	0.003	0.0001	balance
2	**27MnCrB5**	0.28	0.22	1.21	0.026	0.010	0.08	0.39	0.01	0.19	0.017	14	0.016	0.0020	balance
3	**27MnCrB5**	0.27	0.17	1.15	0.017	0.010	0.10	0.35	0.01	0.28	0.019	15	0.016	0.0038	balance
4	**27MnCrB5**	0.27	0.17	1.22	0.014	0.007	0.12	0.34	0.02	0.24	0.019	11	0.017	0.0045	balance

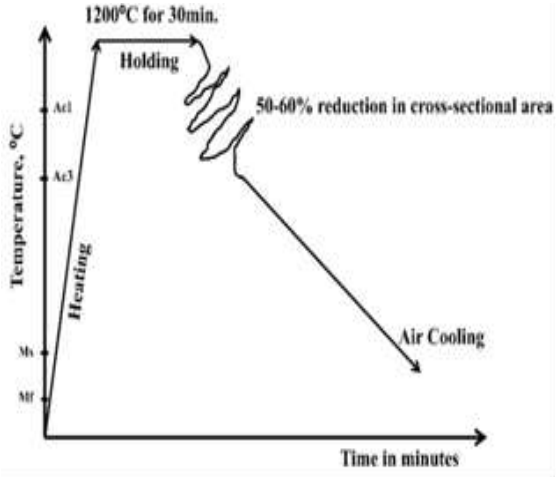

Figure1-Hot-forging process followed by air cooling

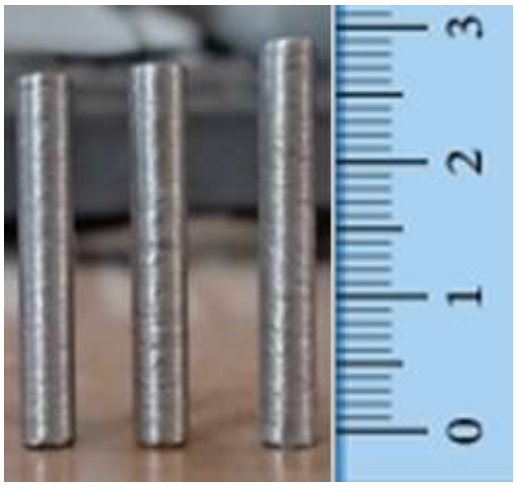

Figure 2- Dilatation samples

Table 2: Actual Critical Transformation Temperatures, °C deduced from dilatation curves.

Alloy	B ppm	Ms	Mf	Md	Bs	Bf	AC1	AC3	Δ Temp. = AC3-AC1
1	1	260	---	278	440	---	727	875	148
2	20	283	---	283	402	---	728	841	113
3	38	302	---	293	451	---	734	828	94
4	45	305	---	331	546	404	737	826	89

3. RESULTS AND DISCUSSION

3.1. Dilatation analysis

Dilatometry is an appropriate experimental technique to estimate the actual transformation data (phase fraction, temperatures, etc.) during heating (or cooling) at a given cooling rate [11]. Figures (4,5,6, and 7) show the dilatation curve in general (showing cooling paths and continuous heating) and the first derivative of dilation during heating and cooling (showing Ac1 and Ac3 temperatures, Bainite and Martensite Zones accurately) for alloys 1,2,3and4, respectively. The dilatometer characterizes the dimensional changes resulting from the transformation of phases as a function of temperature, and that is reflected clearly in the dilatation curves, from which critical transformation temperatures are deduced [12]. The critical transformation temperatures (Ac1, Ac3, Ms, Md, Bs, and Bf) deduced from dilatation Curves are given in Table 2. It is noticed that the increase of boron content makes the intercritcical zones (partial transformation from ferrite to austenite) very narrow due to the decrease of Ac3 and the increase of Ac1 temperatures. Also, martensite starts temperature increases with the increase of boron content. Figure.3 shows CCT diagrams for alloys 1,2,3, and 4 calculated by JMatPro software. The effect of boron is clearly visible as it shifts the C-curves to the right, thereby improving the steel hardenability with a lower quenching rate to avoid quench cracking

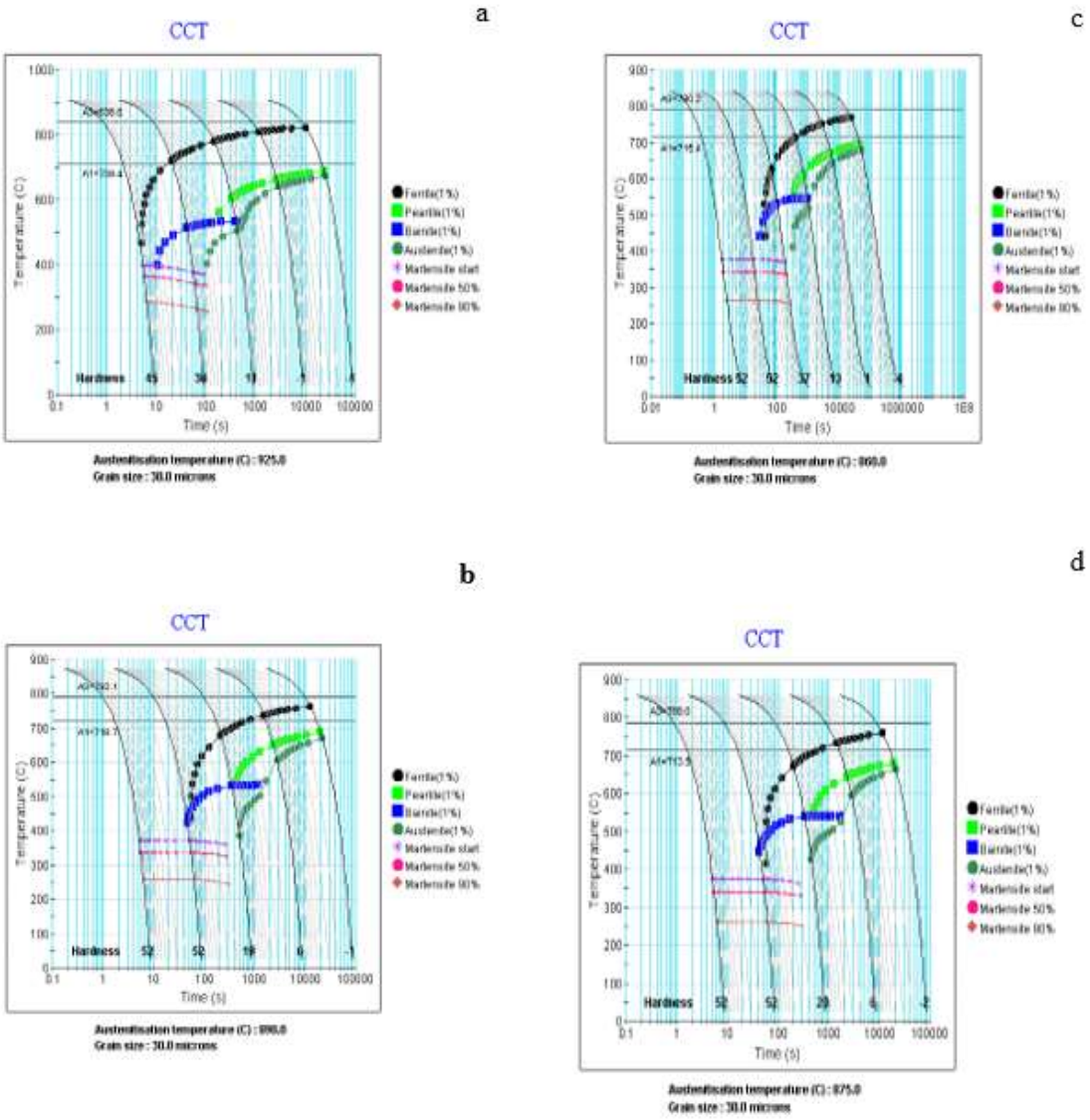

Figure 3- CCT diagrams for a) alloy 1, b) alloy2, c) alloy3 and d) alloy4 calculated by JMatPro software

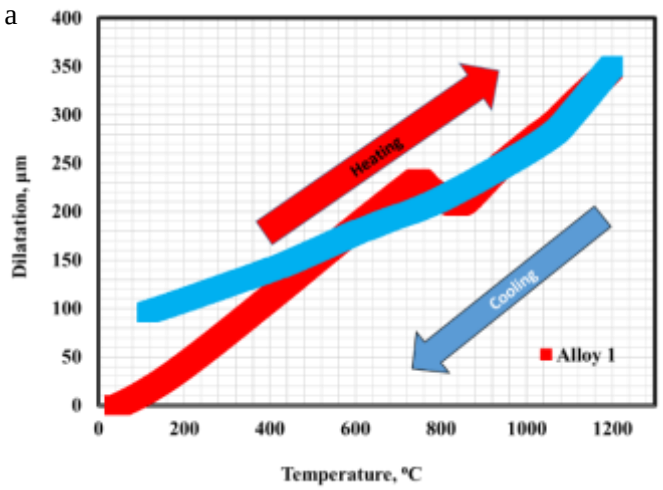

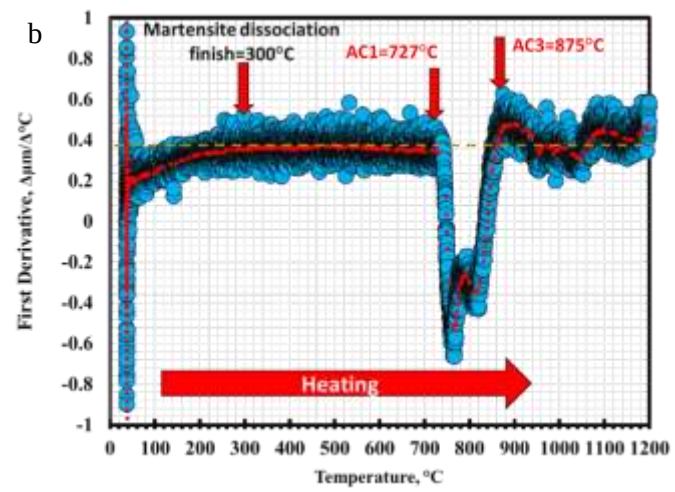

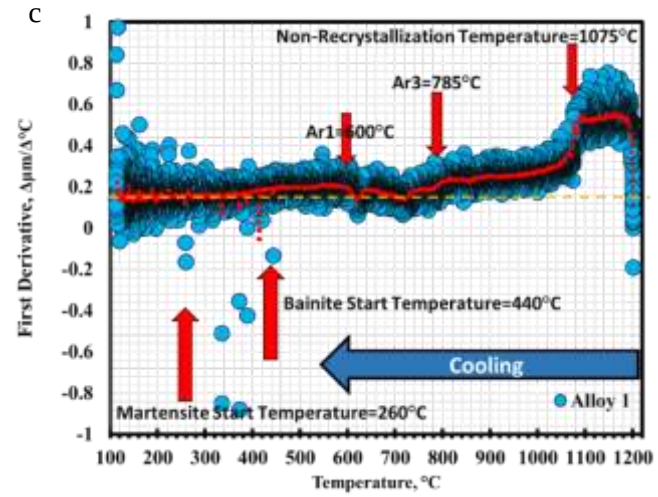

Figure 4- a) Dilatation curve in general (showing cooling paths and continuous heating)
b,c) First Derivative of dilation during heating and cooling respectively for alloy 1 (showing Ac1 and Ac3 temperatures, Bainite and Martensite Zones accurately)

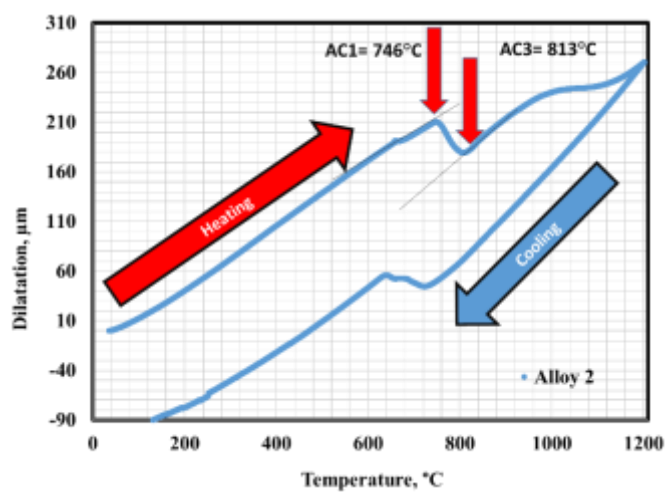

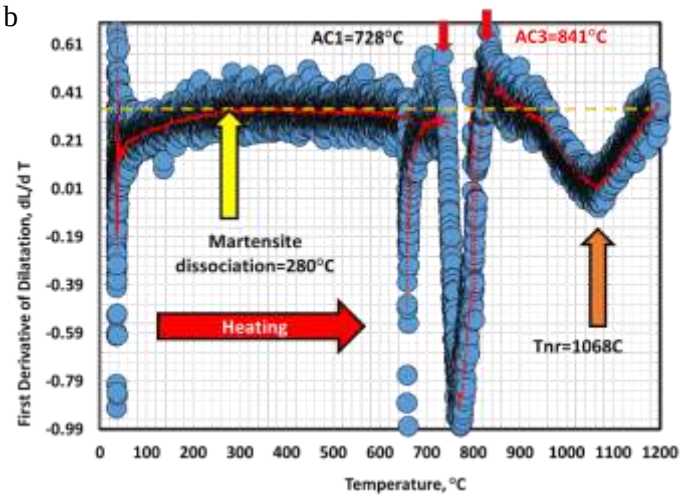

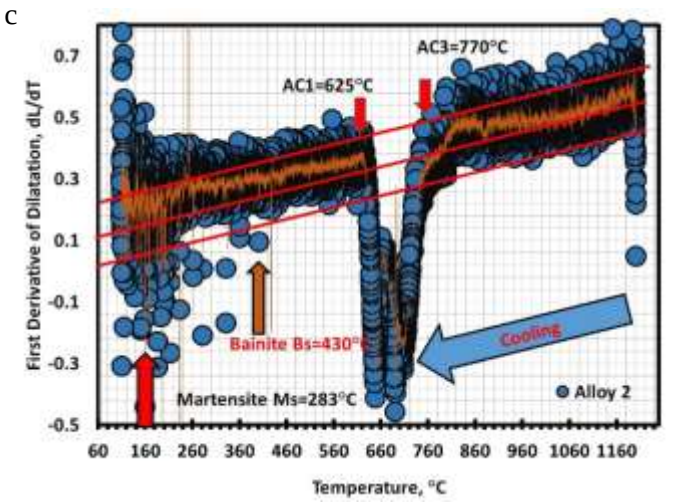

Figure 5- a) Dilatation curve in general (showing cooling paths and continuous heating)
b,c) First Derivative of dilation during heating and cooling respectively for alloy 2 (showing Ac1 and Ac3 temperatures,Bainite a nd Martensite Zones accurately)

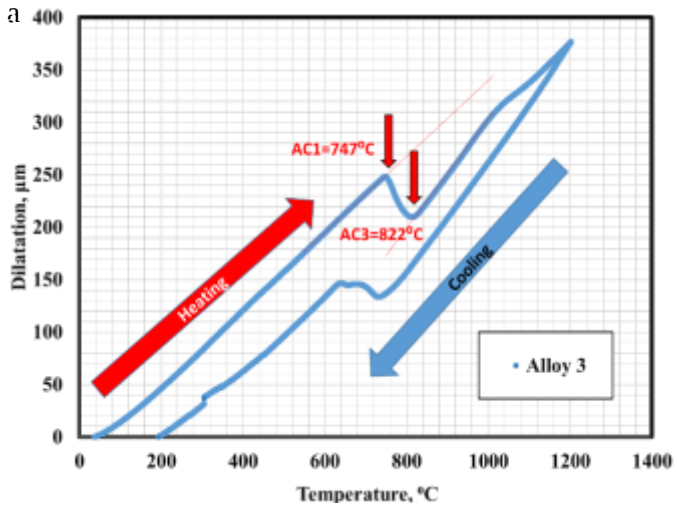

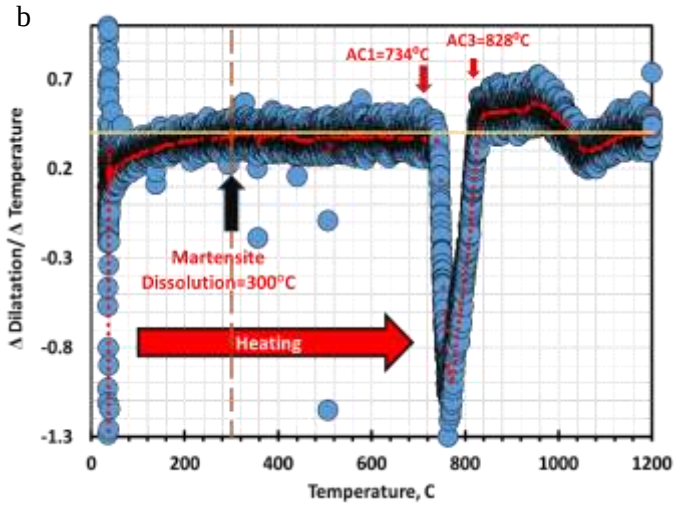

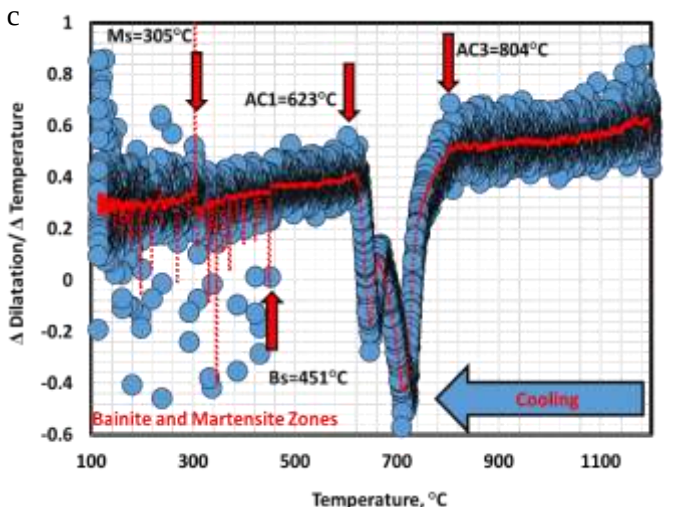

Figure 6- a) Dilatation curve in general (showing cooling paths and continuous heating)

b,c) First Derivative of dilation during heating and cooling respectively for alloy 3 (showing Ac1 and Ac3 temperatures, Bainite and Martensite Zones accurately)

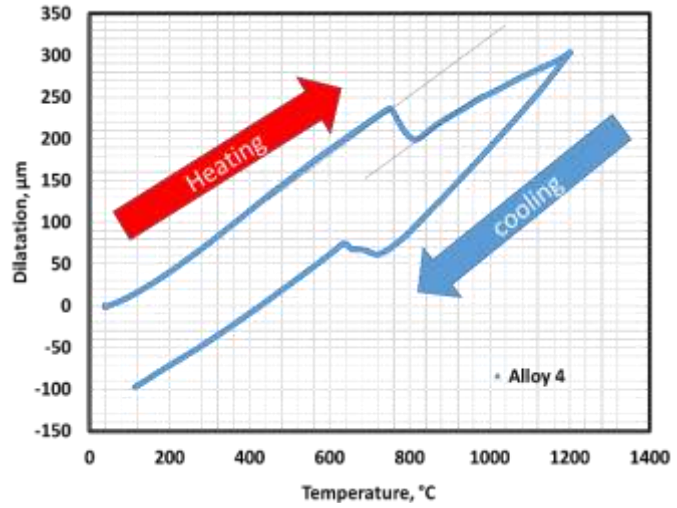

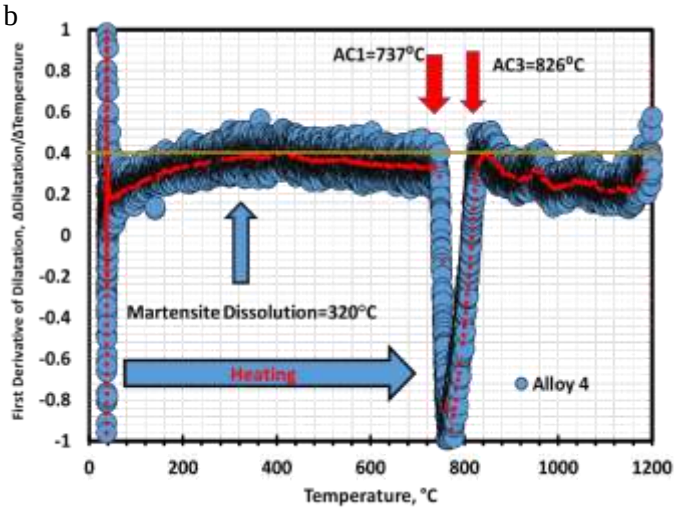

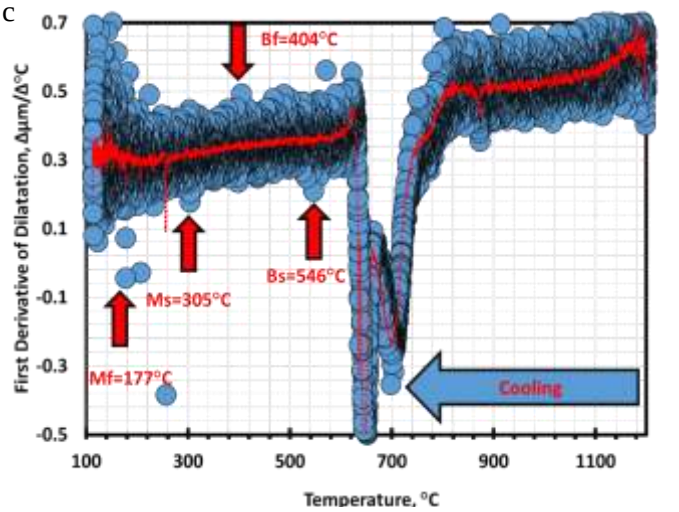

Figure 7- a) Dilatation curve in general (showing cooling paths and continuous heating)

b,c) First Derivative of dilation during heating and cooling respectively for alloy 4 (showing Ac1 and Ac3 temperatures, Bainite and Martensite Zone accurately)

3.2. Microstructure results

The microstructure of the hot-forged alloys will be discussed according to two aspects represented in phase height and thickness.

Figure.8a shows the optical microstructure for alloy 1 that contains 1ppm boron. It has a mixture of ferrite (white color in optical photo) and pearlite phase (dark phase in optical photo). However, the dark phase is expected to be pearlite due to slow cooling. Furthermore, to emphasize the pearlite phase-only, it needs to be investigated using SEM microscopy. Figure. 8b emphasizes the existence of blocky martensite in addition to ferrite (very dark color and low height in SEM) and pearlite (grey color and a little higher than ferrite phase). It is noticed that ferrite grain has a very low height relative to the other phases, while the martensite phase has a very high height, and the pearlite phase is in between. Alloy 2 has a ferrite phase (white color in optical photo) surrounding the pearlite phase (dark phase), as seen in optical Fig.9a. SEM micrographs show islands of pearlite surrounded by ferrite nets, as shown in Fig.9b. The existence of ferrite-pearlite only has not been emphasized. Therefore, Fig.9a shows three phases ferrite, pearlite, and martensite. So, with an increase of boron content, even at a slow cooling rate, the blocky martensite is precipitated. Alloy 3 has a mixture of ferrite (white color) and pearlite phase (dark phase) as seen in optical Fig.10a. it is also noticed that thin layers of ferrite net (black) surrounding the pearlite islands (Grey) as shown in Fig.10b. Furthermore, blocky martensite was more pronounced than alloy 2. Alloy 4 has a ferrite phase (white color) surrounding the pearlite phase (dark phase), as seen in optical Fig.11a. It is found that the blocky martensite increases and its size is bigger than the previous three alloys, as shown in Fig.11b. Figure.12a represents the histogram of the ferrite thickness for a hot-forged (alloy 1) steel containing 1ppm Boron; It shows that the average thickness of ferrite is 5.58µm. Figure. 12b represents the histogram of the ferrite thickness for a hot-forged (alloy 2) steel containing 20ppm boron. It shows that the average thickness of the ferrite is 12.69µm. It is clear that ferrite thickness is getting coarse. Figure.13a represents the histogram of the ferrite thickness for a hot-forged (alloy 3) steel containing 38ppm Boron; It shows that the average thickness of ferrite is 3.43µm. Figure.13b represents the histogram of the ferrite thickness for a hot-forged (alloy 4) steel containing 45ppm Boron; It shows that the average thickness of ferrite is 2.62µm. From previous Figures (1-13), it is clear that boron does encourage the formation of carbide phase (pearlite and martensite) depending on cooling rates and does not support the existence of ferrite. Boron also refines pearlite morphologies and coarsens pearlite islands.

Figure. 14 summarizes the effect of boron content on the ferrite thickness. It seems clear that the ferrite thickness increases with the increase of boron content to 20ppm boron, then the ferrite thickness decreases with the increase of boron content.

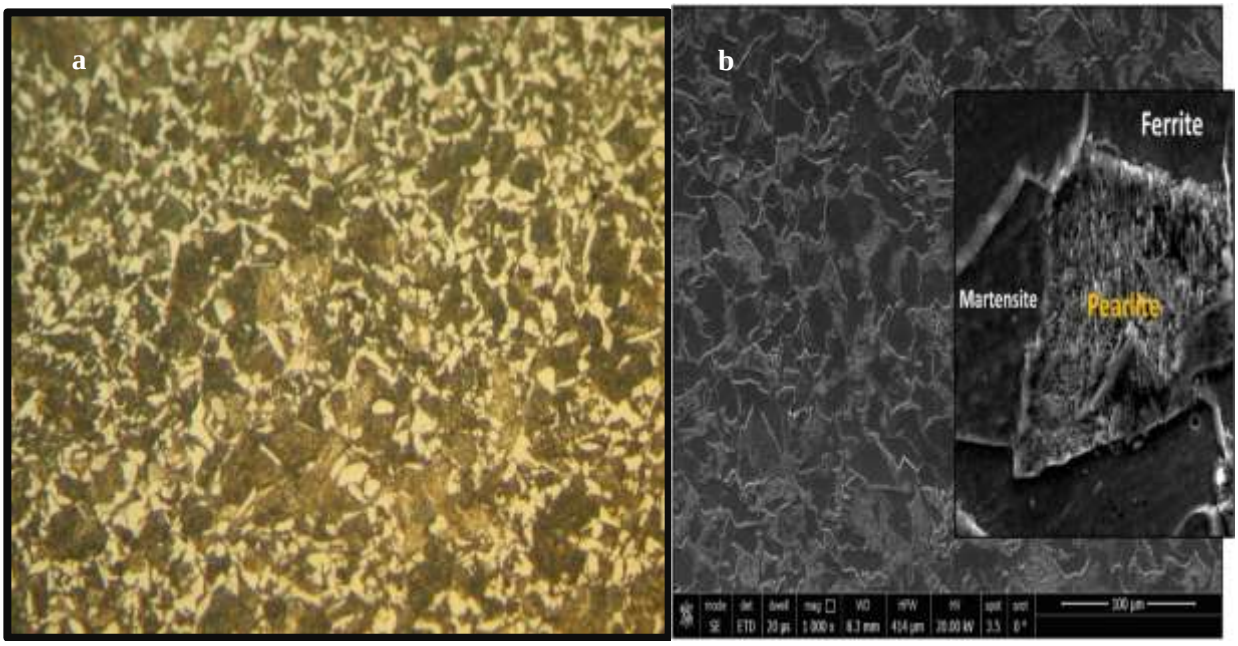

Figure 8 a) Optical Microstructure(500x) b) SEM Microstructure containing ferrite (Black zones) and pearlite (Grey zones) of Alloy 1 containing 1ppm Boron

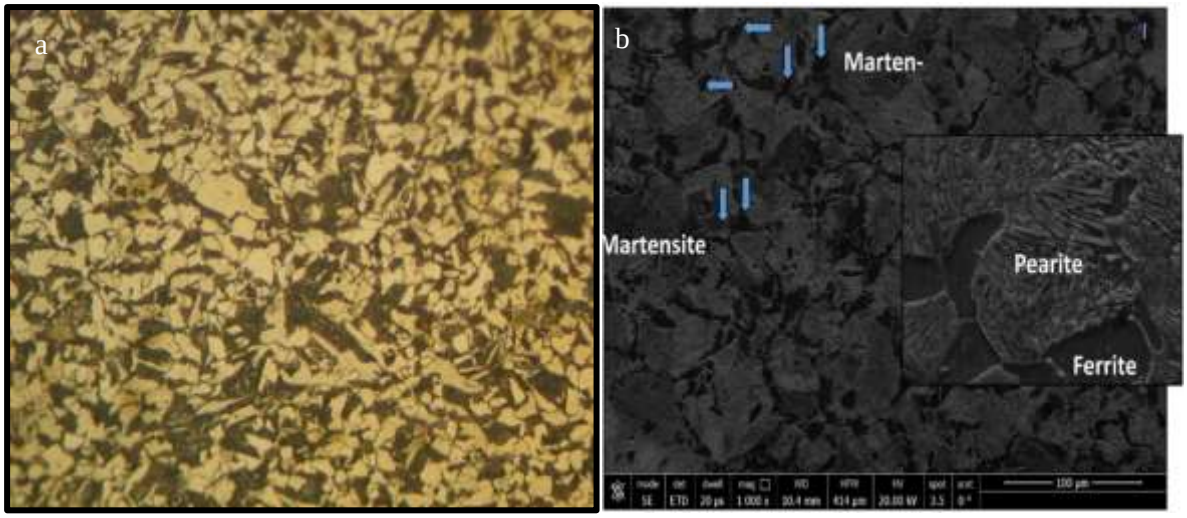

Figure 9- a) Optical Microstructure(500x) b) SEM Microstructure containing the ferrite (Black zones) and pearlite (Grey zones) of Alloy 2 containing 20 ppm Boron

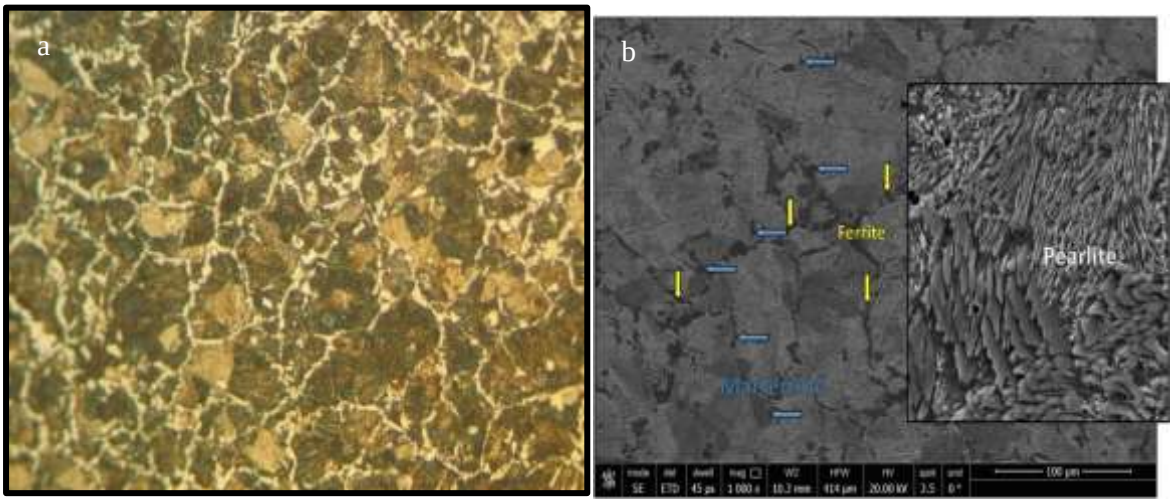

Figure 10- a) Optical Microstructure(500x) b) SEM Microstructure of Alloy 3containing 38ppm Boron

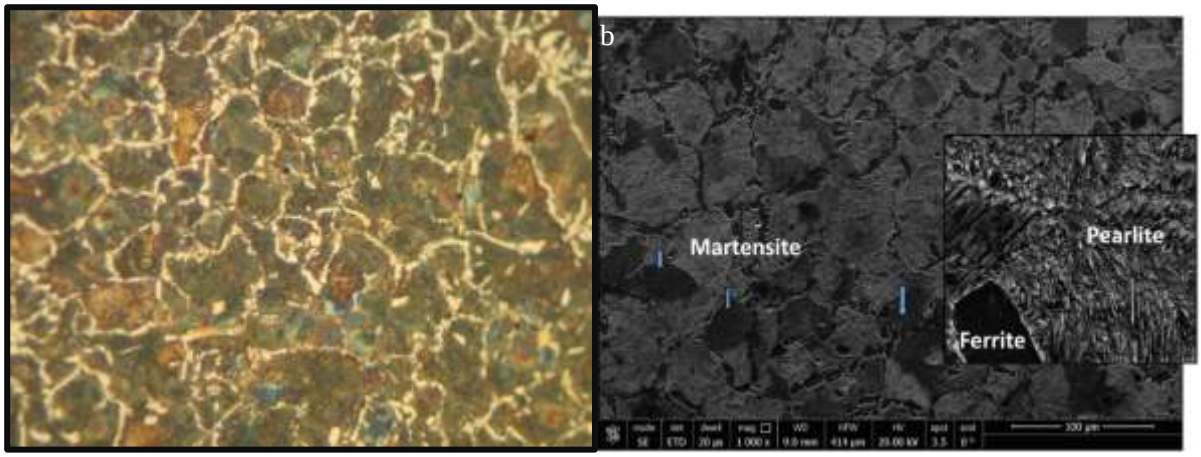

Figure 11- a) Optical Microstructure(500x) b) SEM Microstructure of Alloy 4 containing 45ppm Boron

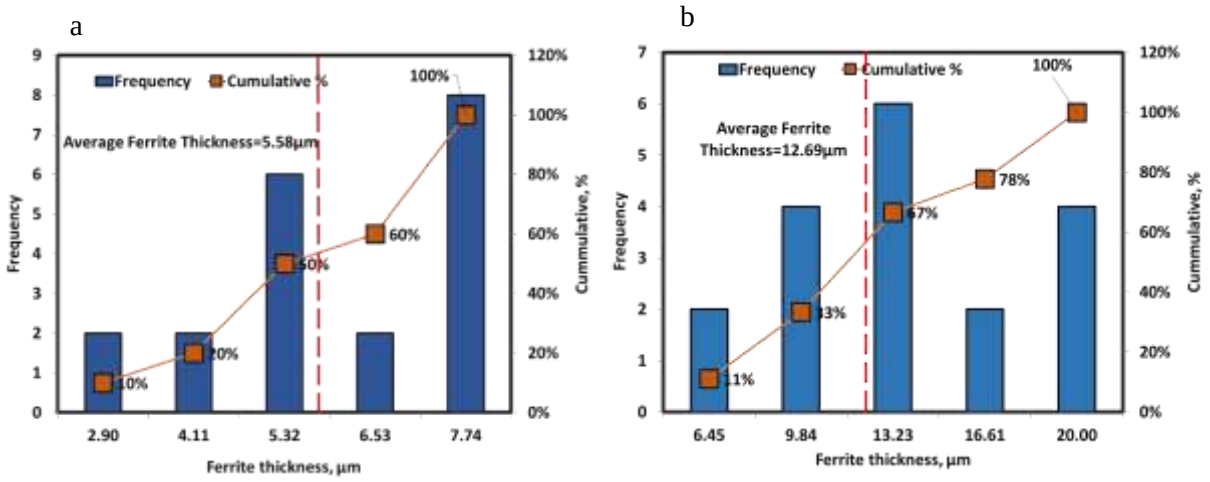

Figure 12- Histogram of ferrite thickness of hot-forged a) alloy 1 b) alloy 2

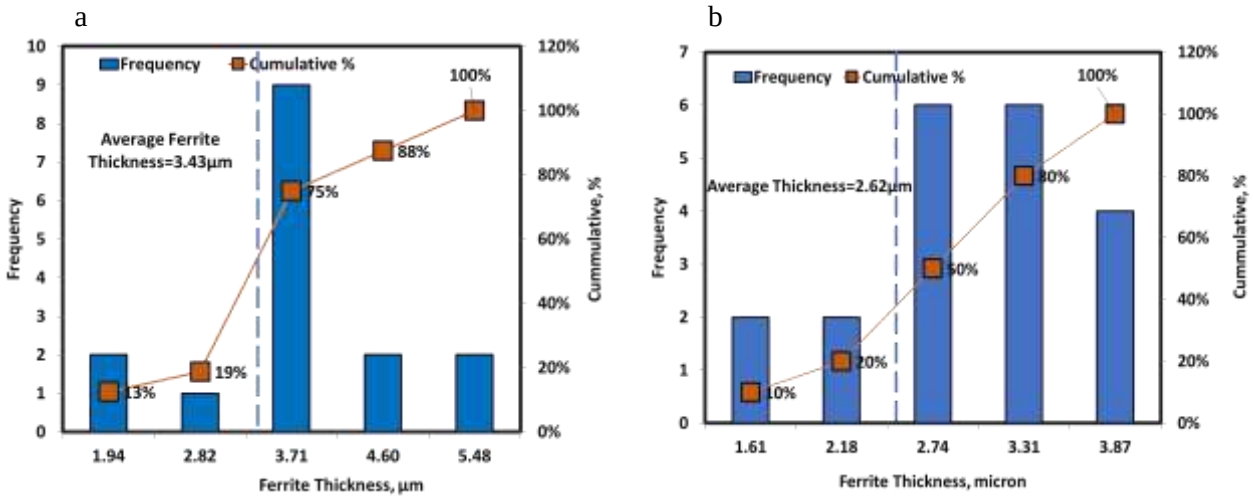

Figure 13- Histogram of ferrite thickness of hot-forged a) alloy 3 b) alloy 4

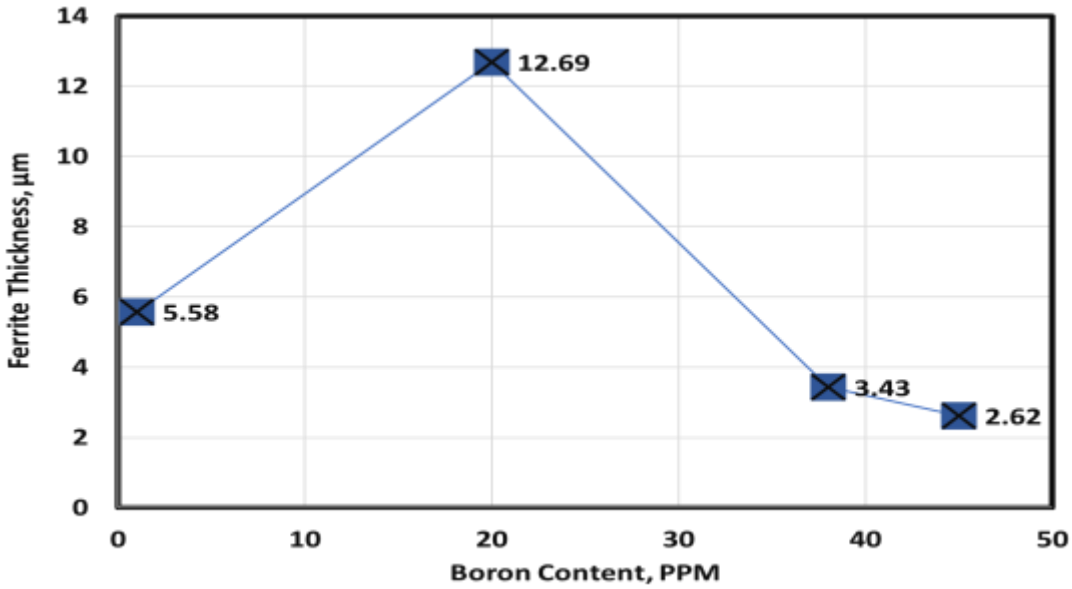

Figure 14- Relationship between boron content and ferrite thickness

3.3. Determination of phases volume fraction using Abbott Firestone Curves

To determine the volume fraction for different phases, a new technique depending on surface roughness deduced from optical or SEM micrographs has been analyzed using MATLAB software. The data obtained from the MATLAB analysis were also statistically analyzed using Excel to conduct the Abbott Firestone curve.

Figures (15a,16a,17a, and 18a) show the average profile of surface roughness for alloys 1,2,3and 4, respectively. It consists of high peaks (martensite), low peaks (ferrite), and mean peaks (pearlite). These figures show only qualitatively the different phases. Meanwhile, Figures (15b,16b,17b, and 18b) belong to the distribution of different surface roughness with their frequencies for alloys 1,2,3and 4, respectively. Each emphasizes three phases but also in a qualitative manner. Figures (15c,16c,17c and 18c) show rose plot of intercept for alloy 1,2,3and 4 respectively. Figures (15d,16d,17d, and 18d) show a rose plot of slope for alloys 1,2,3, and 4, respectively. Rose polts of intercept and slope show different surface roughnesses at different angles within SEM micrographs. However, figures (15,16,17, and 18) show only qualitatively the different phases. Therefore it is necessary to get a quantitative result using MATLAB software to analyze SEM micrographs; then, the results were statistically analyzed using Excel to conduct the Abbott Firestone curve. Figure19.a shows the Abbott Firestone Curve for alloy 1 Analysis to the different phases. It is clear that the ferrite volume fraction is 32%, while the pearlite phase volume fraction is 56, and finally, blocky martensite is 12%. The correlation factor is more than 99% accurate. Figure 19. b shows Abbott Firestone curve for alloy 2; it is noticed that martensite phase volume fraction slightly increased (14%), pearlite phases slightly decreased (48%), while ferrite phase slightly increased (34%). Figure 19. c is Abbott Firestone curve for alloy 3; it is noticed that martensite has the same volume fraction of martensite (13%), pearlite phases slightly increased (73%) while ferrite phase slightly decreased (14%). Figure 19.d describe the Abbott Firestone curve for Alloy 4. To emphasize the results of the ferrite phase (white in the optical photo), ImageJ software was used to calculate the ferrite volume fraction; It was found about 36% for alloy1 is very near to the Abbott Firestone results in Fig. 20. Figure. 21 shows the ferrite volume fraction of alloy 2 using ImageJ software; It is clear that the ferrite phase is about 30% near to the result of the Abbott Firestone Curve. Figure.22 shows the ferrite volume fraction of alloy 3 using ImageJ software. It is clear that the ferrite phase is about 12%, very near the Abbott Firestone Curve result. Figure. 23 indicates the volume fraction of the ferrite phase (12.5%) of alloy 4. Figure.24 indicates the correlation factor is 95% accuracy between Ferrite volume fraction using Abbott technique results and ImageJ software results. Thereby Abbott Firestone curve technique results are reliable and very close to that Image j software results with a percentage of 95%. Figure. 25 summarizes the effect of boron content on ferrite, pearlite, and blocky martensite. Generally, at a high level of boron, pearlite is encouraged while blocky martensite and ferrite are not increased. However, at a low level of boron, pearlite and ferrite are encouraged at the expense of martensite. Martensite has a constant volume fraction except for alloy 4 (45ppm boron).

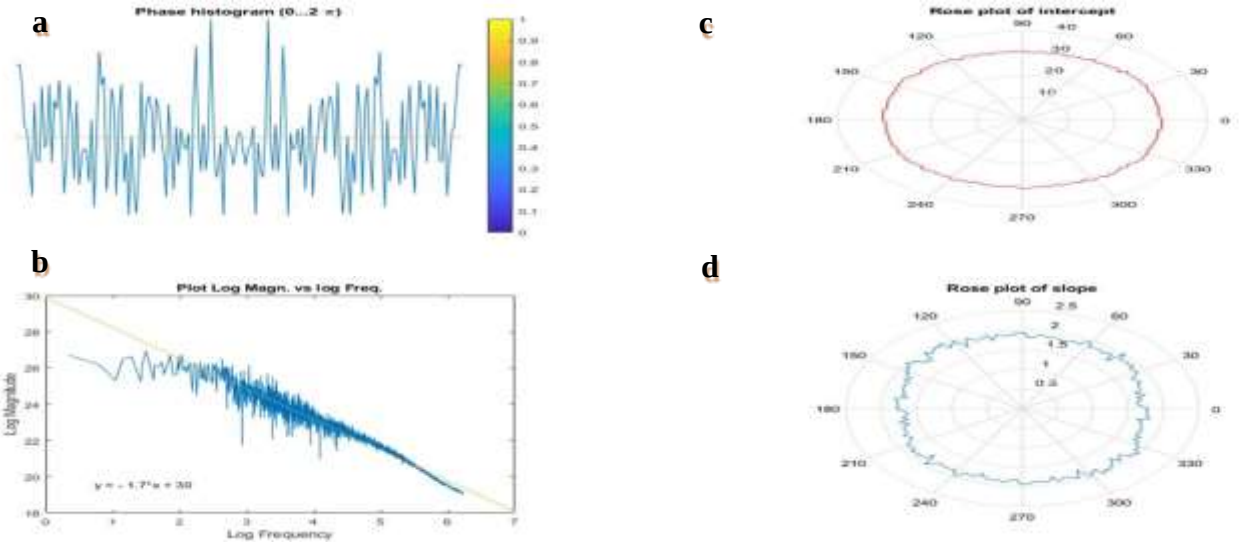

Figure 15- a) mean (average) surface roughness profile, - (b) distribution of different surface roughness with its frequency - (c) rose plot of intercept - (d) rose plot of slope for alloy 1

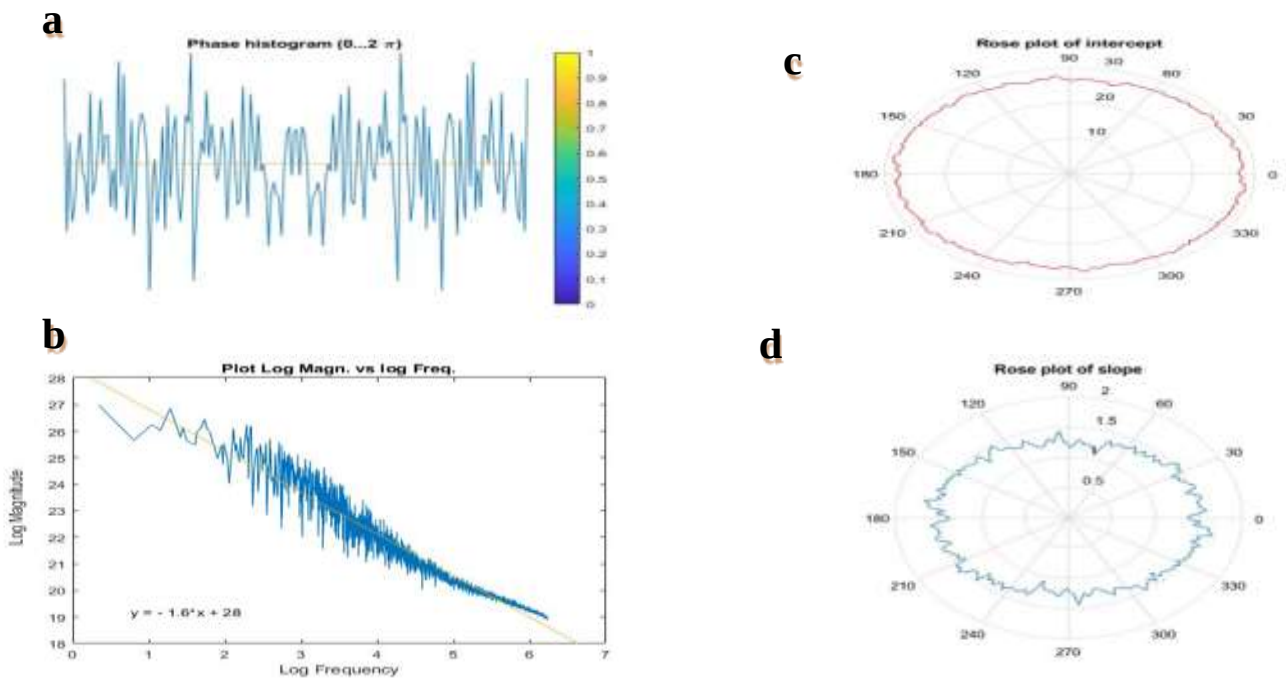

Figure 16- a) mean (average) surface roughness profile - (b) distribution of different surface roughness with its frequency - (c) rose plot of intercept - (d) rose plot of slope for alloy 2

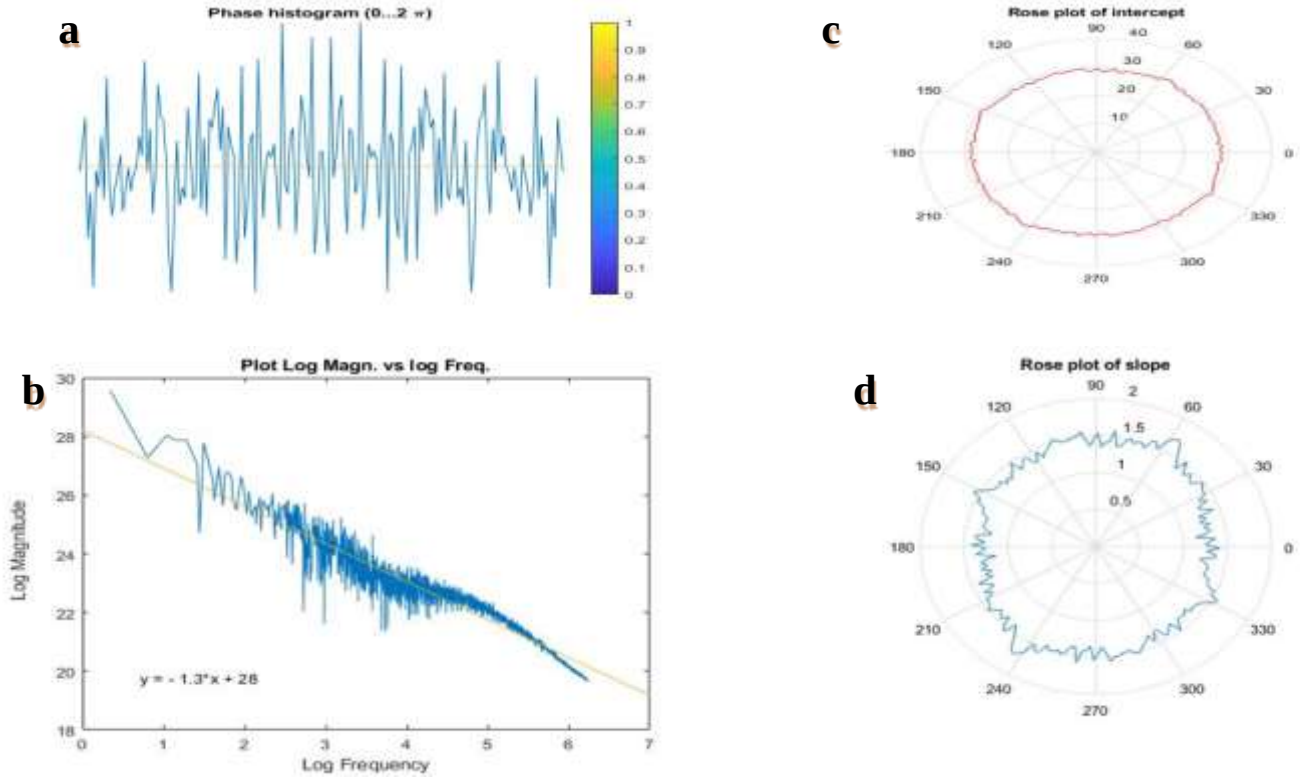

Figure 17- a) mean (average) surface roughness profile - (b) distribution of different surface roughness with its frequency - (c) rose plot of intercept - (d) rose plot of slope for alloy 3

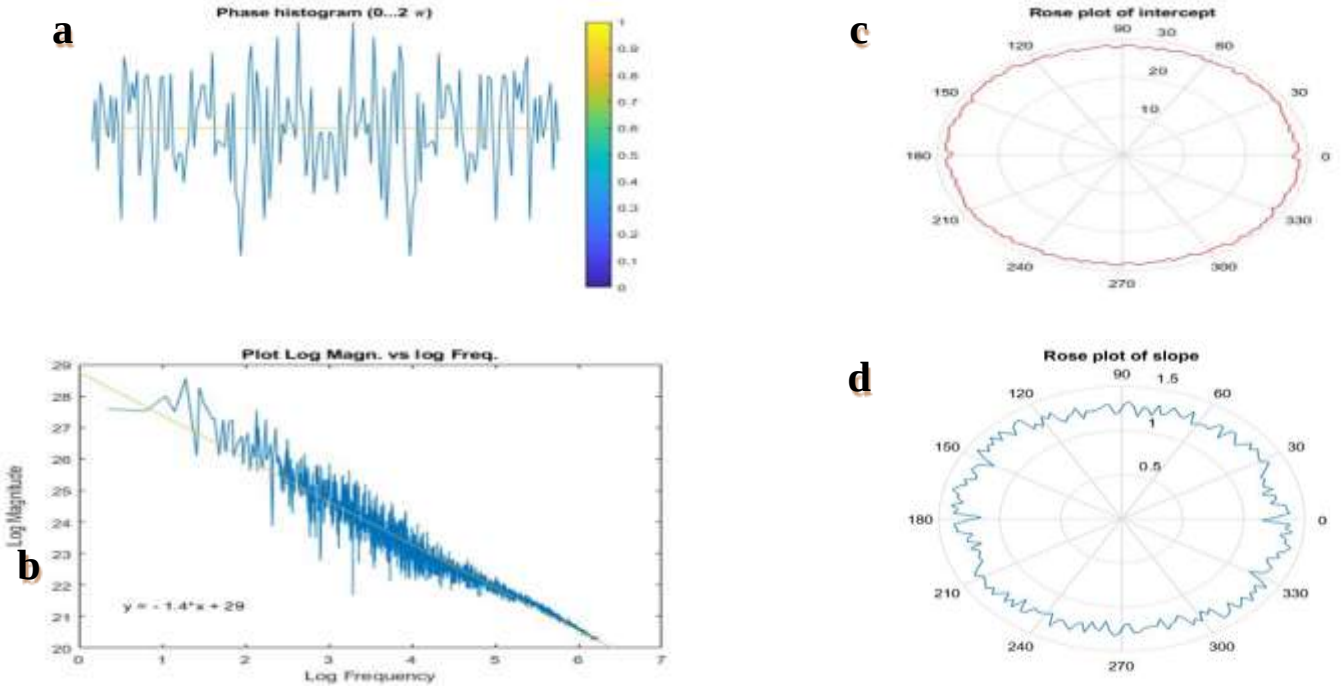

Figure 18- a) mean(average) surface roughness profile, (b) distribution of different surface roughness with its frequency, (c) rose plot of intercept, and (d) rose plot of slope for alloy 4

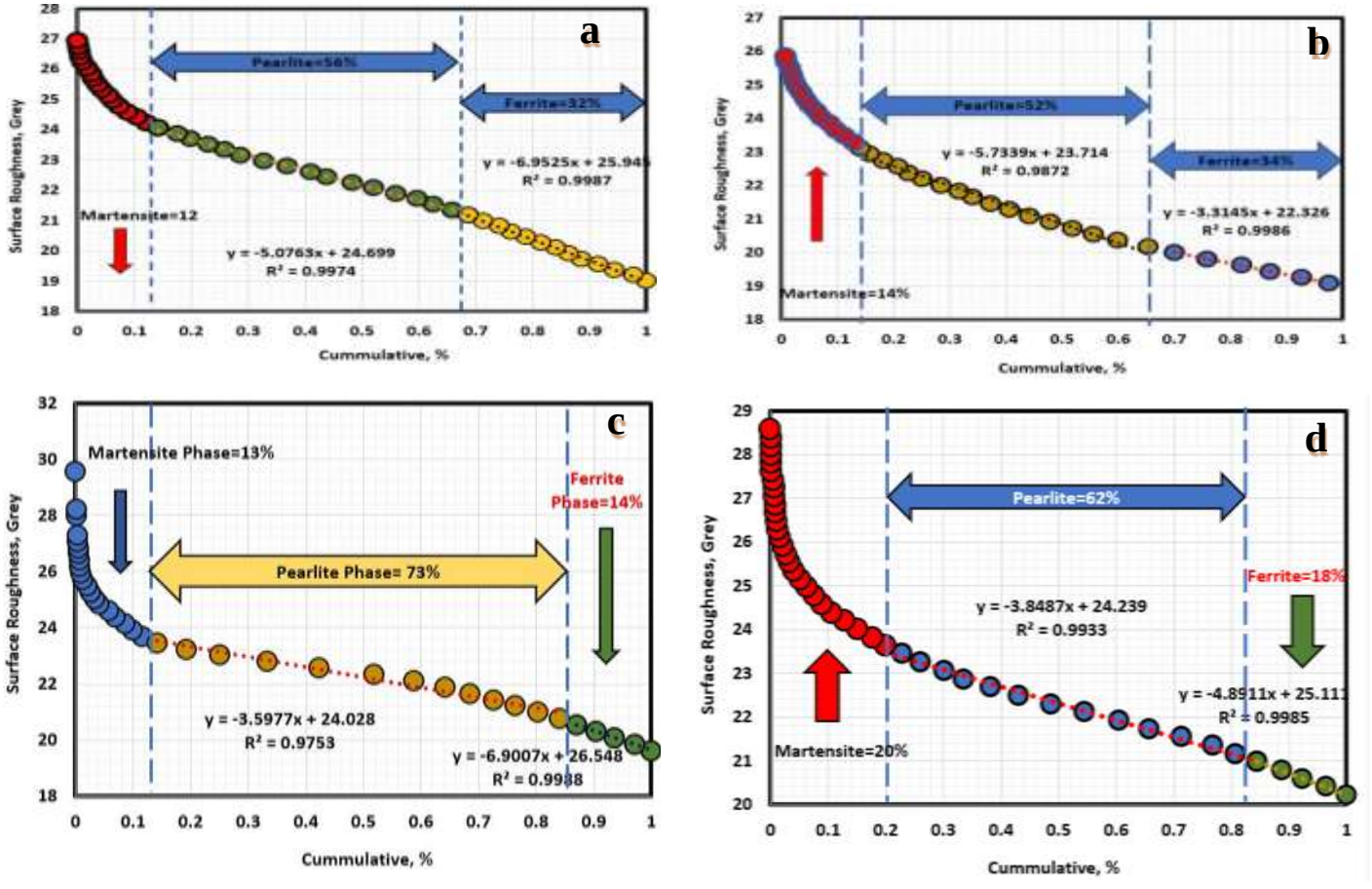

Figure 19- Abbott Firestone curve for a) alloy 1 - b) alloy 2 - c) alloy 3 - d) alloy 4 hot-forged

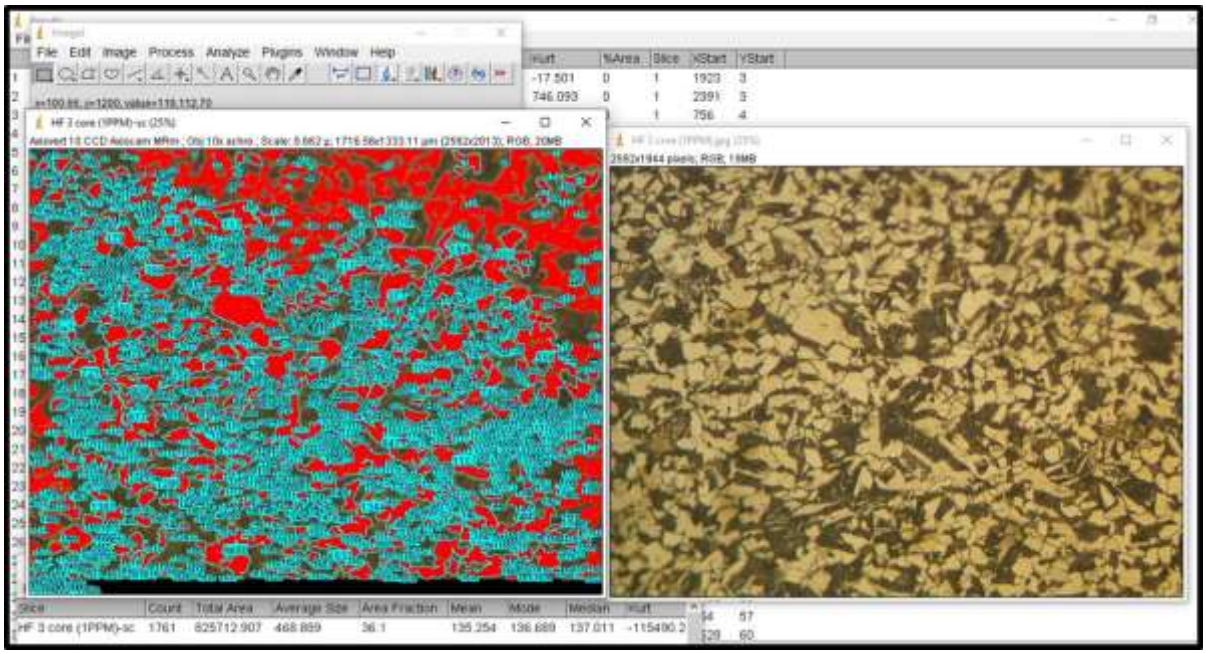

Figure 20- Ferrite phase volume fraction using the ImageJ software for Alloy 1

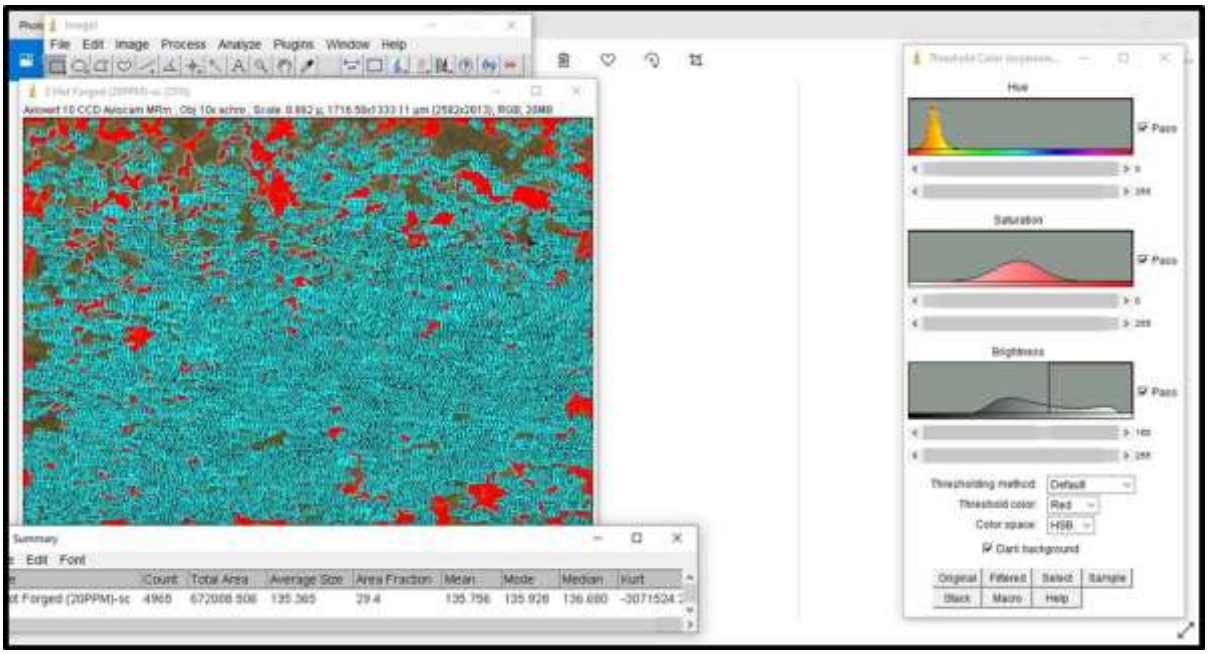

Figure 21- Ferrite phase volume fraction using the ImageJ software for Alloy 2

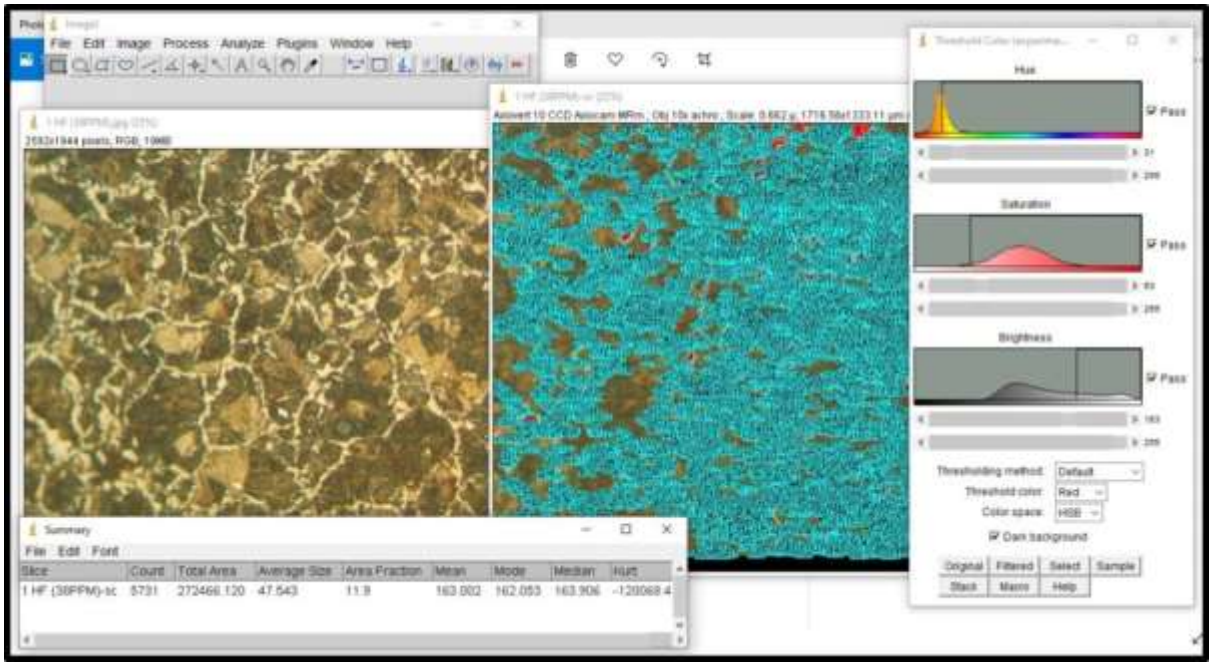

Figure 22- Ferrite phase volume fraction using the ImageJ software for Alloy 3

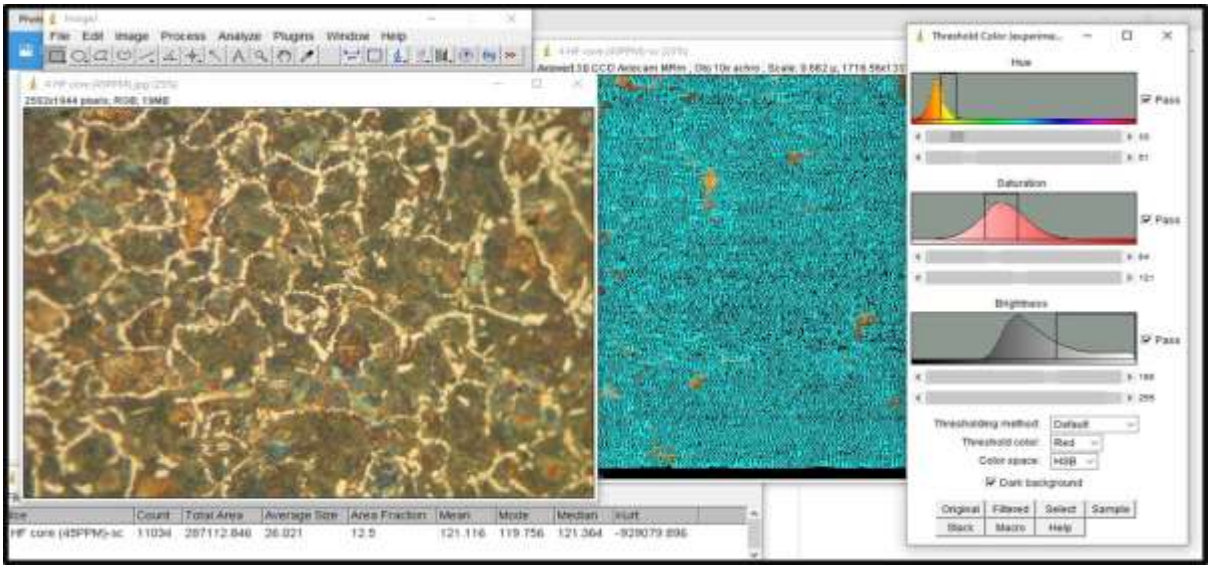

Figure 23- Ferrite phase volume fraction using the ImageJ software for Alloy 4

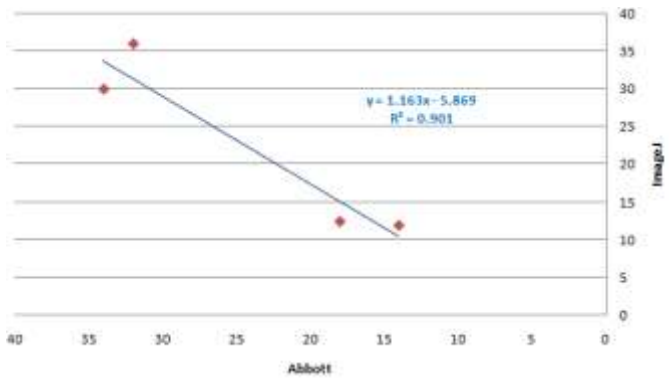

Figure 24- Correlation between Abbott technique results and the ImageJ software results (R=0.95)

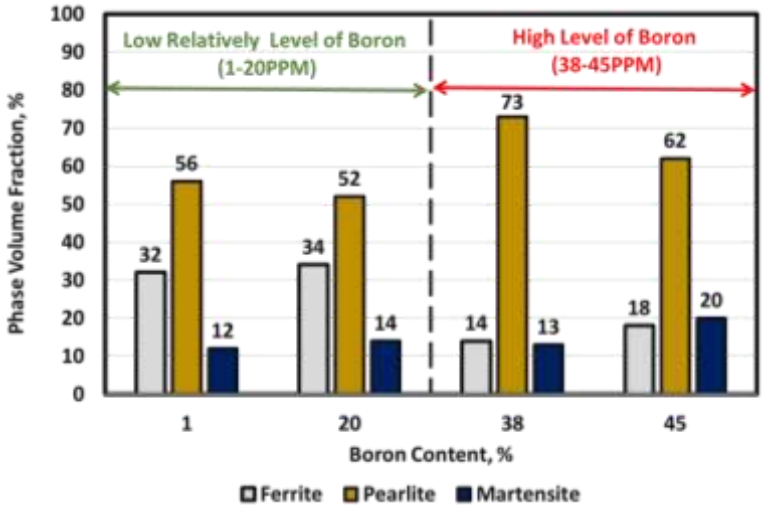

Figure 25- Relationship between boron content and "ferrite, pearlite, and martensite" phase volume fraction

3.4. Tensile properties of hot-forged steel

Discontinuous yielding is a special form of yielding wherein the elastic-plastic transition occurs abruptly with a drop in stress and is followed by the propagation of a Lüders band manifesting itself in the appearance of serrations in the stress-strain curve. Carbon and/or nitrogen atoms locked the Dislocations [13]. When locked dislocations are set free and/or new dislocations are propagated, the Lüders band spreads, causing industrial problems such as that happened in the drawing and stamping operations by generating a rough appearance on the metal sheet's surface.

Therefore, to avert discontinuous yielding, alloying elements, such as titanium, boron and/or niobium were added, it is desirable to lower the amount of carbon and nitrogen in solution through the formation of stable nitrides and/or carbides [14]. Figure.26 describes the engineering stress-strain behavior of the four alloys. The effect of increasing boron on discontinuous yielding is clear where boron up to 20ppm exhibits discontinuous yielding, beyond which boron produces continuous yielding.

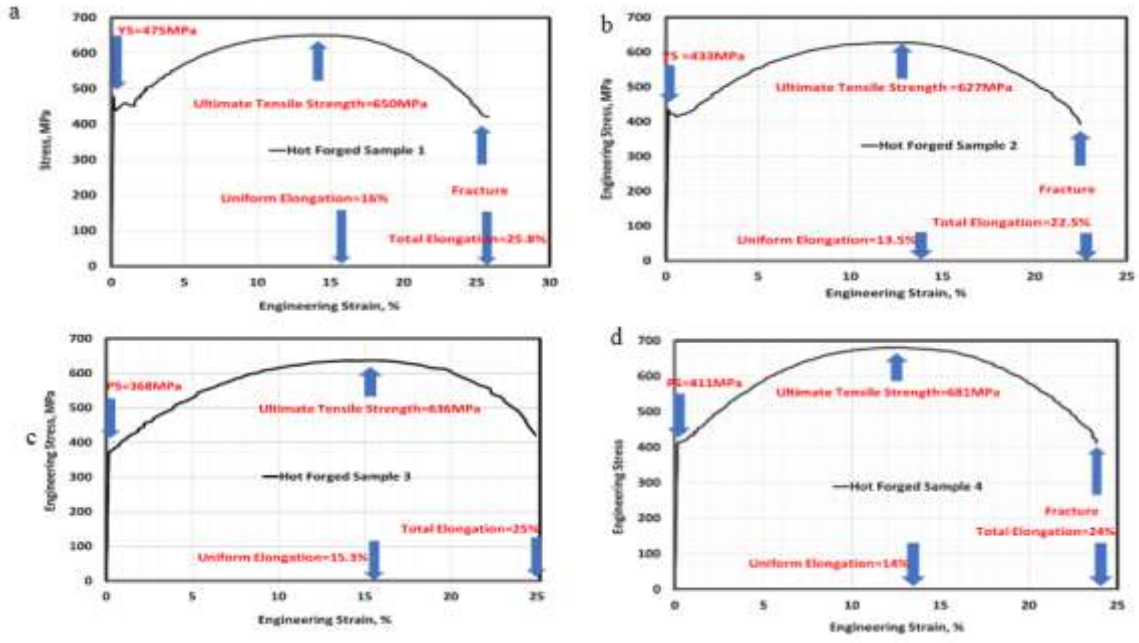

Figure 26- Engineering stress-strain diagrams of a) alloy1 b)alloy2 c)alloy3 d)alloy 4

4. CONCLUSIONS

1. It is noticed that increasing boron content makes intercritcical zones (partial transformation from ferrite to austenite) very narrow due to decreasing AC3 and increasing AC1 temperatures.
2. Martensite starts temperature increases with the increase of boron content.
3. Boron does encourage the formation of pearlite at moderately cooling rates and does not support the existence of ferrite. Boron also refines pearlite morphologies and coarsens pearlite.
4. Ferrite thickness increases with increasing boron content up to 20ppm, beyond which the ferrite thickness decreases with increasing boron content.
5. At high levels of boron, pearlite is encouraged, while blocky martensite and ferrite have not been increased. However, at a low level of boron, pearlite and ferrite are encouraged at the expense of martensite. Martensite has almost a constant volume fraction except for alloy 4 (45ppm boron).
6. The Abbott Firestone curve technique results are reliable and very close to Image j software results with a percentage of 95%. Based on that, this method facilities the prediction of steel phases volume fraction related to surface roughness, which will be fruitful for engineers in the field of steel manufacturing.
7. Boron up to 20ppm exhibits a discontinuous yielding beyond which boron produces a continuous yielding

5. ACKNOWLEDGMENT

Special thanks to (ARCOSTEEL) company for generous support. Continuous guidance and encouragement provided by chemist / Said E. Monier (SMP manager) and engineer / Radi Nasr (production sector manager) is also appreciated.

6. References

[1] Llewellyn DT, Cook WT. Metallurgy of boron-treated low-alloy steels. Metals Technology. 1974 Jan 1;1(1):517-29.

[2] KnowltonHB. American applications of boron and other low-alloy steels. Journal of the Iron and Steel Institute. 1954 Jan 1;176(2):187.

[3] Sharma M, Ortlepp I, Bleck W. Boron in Heat Treatable Steels: A Review. Steel research international. 2019 Nov;90(11):1900133.

[4] Deva A, De SK, Kumar V, Deepa M, Jha BK. Influence of boron on the hardenability of unalloyed and low alloyed steel. International Journal of Metallurgical Engineering. 2013;2(1):47-51

[5] Opiela M. Effect of thermomechanical processing on the microstructure and mechanical properties of Nb-Ti-V microalloyed steel. Journal of Materials Engineering and Performance. 2014 Sep;23(9):3379-88.

[6] Korobeinikov I, Chebykin D, Seetharaman S, Volkova O. Effect of boron micro-alloying on the surface tension of liquid iron and steel alloys. International Journal of Thermophysics. 2020 May;41(5):1-4.

[7] Jahazi M, Eghbali B. The influence of hot forging conditions on the microstructure and mechanical properties of two microalloyed steels. Journal of Materials Processing Technology. 2001 Jun 15;113(1-3):594-8.

[8] Zrnik J, Kvackaj T, Pongpaybul A, Sricharoenchai P, Vilk J, Vrchovinsky V. Effect of thermomechanical processing on the microstructure and mechanical properties of Nb–Ti microalloyed steel. Materials Science and Engineering: A. 2001 Dec 1;319:321-5.

[9] Salcedo MC, Coral IB, Ochoa GV. Characterization of surface topography with Abbott Firestone curve. Contemporary Engineering Sciences. 2018;11(68):3397-407.

[10] Rîpă M, Tomescu L, Hapenciuc M, Crudu I. Tribological characterisation of surface topography using Abbott-Firestone curve. Annals of University Dunărea de Jos of Galati, Fascicle VIII, Tribology. 2003 Sep 24:208-12.

[11] Ranjan R, Singh SB. Formation of austenite in steels during heating: analysis of dilatation data. Materials Science and Technology. 2019 May 3;35(7):782-90.

[12] Ranjan R, Singh SB. Bainite transformation during Continuous cooling: analysis of dilatation data. Metallurgical and Materials Transactions A. 2018 Jan;49(1):88-93.

[13] Takaki S, Akama D, Nakada N, Tsuchiyama T. Effect of grain boundary segregation of interstitial elements on Hall–Petch coefficient in steels. Materials Transactions. 2014 Jan 1;55(1):28-34.

[14] Wang Y, Tomota Y, Ohmura T, Gong W, Harjo S, Tanaka M. Continuous and discontinuous yielding behaviors in ferrite-cementite steels. Acta Materialia. 2020 Sep 1;196:565-75.